

The Status and Performance of H.E.S.S.

Wystan Benbow for the H.E.S.S. Collaboration

Max-Planck-Institut für Kernphysik, P.O. Box 103980, D 69029 Heidelberg, Germany

Abstract. The High Energy Stereoscopic System (H.E.S.S.) is an array of four imaging air-Cherenkov telescopes located in the Khomas Highlands of Namibia ($23^{\circ} 16' 18''$ S, $16^{\circ} 30' 1''$ E, 1835 m above sea level). Construction of H.E.S.S. Phase-1 is complete as of December 2003. Although under construction, H.E.S.S. has been operating since June 2002, with observations using increasing numbers of telescopes as they became available. The good angular resolution and background rejection provided by the stereoscopic technique give H.E.S.S. a low energy threshold (~ 100 GeV) and allows the detection of a 1% Crab flux source in ~ 25 hours of observation. This sensitivity is unprecedented and has enabled H.E.S.S. to detect numerous new sources of astrophysical gamma-rays. Further details regarding the status and performance of H.E.S.S. are reported here.

THE H.E.S.S. DETECTOR

The H.E.S.S. detector consists of a system of four identical telescopes arranged in a square of 120 m side. Each individual telescope is an alt-az mount Davies-Cotton reflector with a flat-to-flat width of 13 m, and has a camera mounted at the focal length of 15 m. The total mirror area of each telescope is 107 m^2 , segmented into 382 individual round (60 cm diameter) front-aluminized glass mirrors. The optics are of good quality resulting in a small point spread function (width $< 0.1^{\circ}$) across the whole field of view. The H.E.S.S. cameras are modular in design and contain all the necessary electronics for operation, triggering, and readout. Each camera contains 960 individual photomultiplier (PMT) pixels subtending 0.16° each, with Winston cone light concentrators. This provides a 5° field of view with a uniform response, and combined with the small angular resolution ($< 0.1^{\circ}$) of H.E.S.S. allows for detailed studies of source morphology and surveys for unknown sources. The trigger electronics divide the camera into overlapping 64 PMT sectors with a trigger requirement that a sector has a minimum number of pixels (3) with a signal above a threshold (5.3) in photoelectrons (PEs) coincident in an effective ~ 1.3 ns trigger window. Once a camera has triggered (~ 800 Hz), a signal is sent out via an optical fiber to a central trigger system [5] which allows for a multiple telescope coincidence requirement. This multiplicity requirement (2 telescopes) significantly reduces the number of triggers from muons and allows for a lower energy threshold by reducing the overall system rate (~ 300 Hz) while maintaining a low system dead time. An online analysis of H.E.S.S. data is also operational and allows for a quick (within ~ 1 hour) look at the data to see if a source has been detected, potentially increasing the science yield of the experiment. More details on H.E.S.S. can be found in Bernlöhr *et al.* [4]; Hofmann [6]; Vincent *et al.* [8].

H.E.S.S. observations are generally taken in 28 minute runs using *Wobble* mode, where the source direction is positioned $\pm 0.5^{\circ}$ in declination relative to the center of the field

of view (f.o.v) of the camera. The direction of the offset is alternated in successive scans to reduce systematic effects. Due to the large field of view and uniform response of the H.E.S.S. cameras, use of *Wobble* mode allows for both on-source observations and simultaneous estimation of the background induced by charged cosmic rays, since the background can be estimated from different regions in the same field of view. This eliminates the need for off-source observations and therefore improves the observational efficiency. The large f.o.v. of H.E.S.S. also allows for improvements in background estimation. A typical method for estimating the background, described in Masterson *et al.* [7], uses a larger area ($\sim 7\times$) than the on-source region, thereby reducing the relative statistical error on the background measurement. Before analysis, all H.E.S.S. data must first pass conservative run selection criteria which remove runs for which the sky was not clear and where the telescopes were not operating within specified requirements (e.g., trigger rate stability, more than 95% of the camera pixels operational).

EVENT RECONSTRUCTION

The analysis of the data passing the run selection criteria proceeds in the following steps: First the images are calibrated [3] and then “cleaned” to remove noise. The image cleaning is done using a two-stage tail-cut procedure which requires a pixel to have a signal greater than 10 PEs and a neighboring pixel to have a signal larger than 5 PEs. Also pixels greater than 5 PEs are included if they have a neighbor greater than 10 PEs. After this image cleaning is performed, the moments of the shower image are parameterized using a Hillas-type analysis. The shower geometry is reconstructed using the intersection of image axes [1] with a typical angular resolution of $\sim 0.1^\circ$ and an average accuracy of ~ 10 m in the determination of the shower core location. To ensure that the analyzed images are not truncated by the edge of the camera, only images which pass a distance cut requiring the image center of gravity to be less than 2° from the center of the camera are used in the reconstruction. At present, at least two telescopes are each required to exceed a minimum total signal (80 PEs) and pass the distance criteria to ensure that the images are well reconstructed.

The energy of observed gamma rays, E_{fit} , is calculated using the mean of the energies estimated for each telescope with a typical event resolution of $\sim 15\%$. Each of the individual energy estimates use the image size, impact parameter of the event, and the zenith angle of observation. The energy estimates are based on the results of Monte Carlo gamma-ray simulations. In the determination of energy spectra only events for which the average bias in E_{fit} is less than 10% are used, effectively placing energy threshold on suitable events. This is done to eliminate any systematic effects that might arise because energy estimates for events near the trigger threshold yield, on average, too large an energy. This energy threshold for spectroscopic studies is only slightly higher than the energy threshold of detected gamma-rays discussed later.

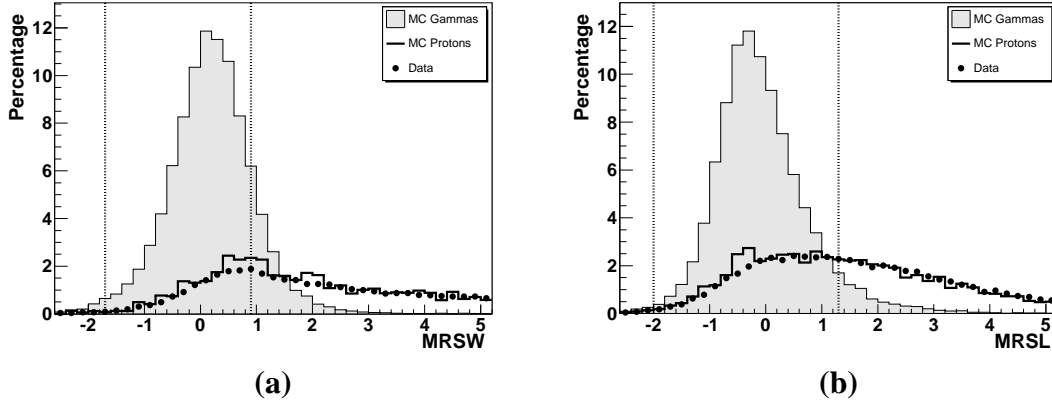


FIGURE 1. The distributions of **a)** mean reduced scaled width (MRSW), **b)** mean reduced scaled length (MRSL) for Monte Carlo gamma-ray simulations (spectral index $\Gamma = 2.59$), Monte Carlo proton simulations ($\Gamma = 2.70$), and actual off-source data. All the distributions are at zenith angle = 20° .

BACKGROUND REJECTION

After the event reconstruction, the much more numerous cosmic-ray background events are rejected using cuts on the parameters mean reduced scaled width (MRSW) and length (MRSL). These parameters are defined as the mean of the difference in standard deviations for each telescope of the width (length) observed in the image from that which is expected from gamma-ray simulations ($\langle \text{width} \rangle$ and σ) based on image intensity, reconstructed impact parameter and the zenith angle of observations. MRSW is defined as:

$$MRSW = \frac{1}{N_{\text{tel}}} \sum_{i=0}^{N_{\text{tel}}} \frac{\text{width}_i - \langle \text{width} \rangle_i}{\sigma_i}, \quad (1)$$

and similarly for MRSL. Figure 1 shows the distributions of MRSW and MRSL for Monte Carlo gamma-ray simulations, Monte Carlo proton simulations, and off-source data. As required, the simulated proton and real cosmic ray (dominated by protons) distributions match well, illustrating that the response of H.E.S.S. is well simulated. The ability to remove the majority of background events while retaining a large fraction of gamma-ray events is also clear. The cuts on MRSW and MRSL used to reject the background events are shown by the vertical lines in Figure 1. Additionally, a cut on the square of the angular difference between the reconstructed shower position and the source position ($\theta^2 < 0.02$) is applied and is equivalent to placing the data into a circular bin centered on the source position. All the cuts are optimized *a priori* (simultaneously) to yield the maximum expected significance per hour of observation. The data used for optimization consists of Monte Carlo gamma-ray simulations at a zenith angle of 20° with a Crab-like energy spectrum ($\Gamma=2.6$, 0.1 Crab flux) and real off-source data. The cuts retain $\sim 40\%$ gamma-rays and $\sim 0.024\%$ of the cosmic rays. The significance expected (and observed) is not strongly dependent on the exact values of the cuts used.

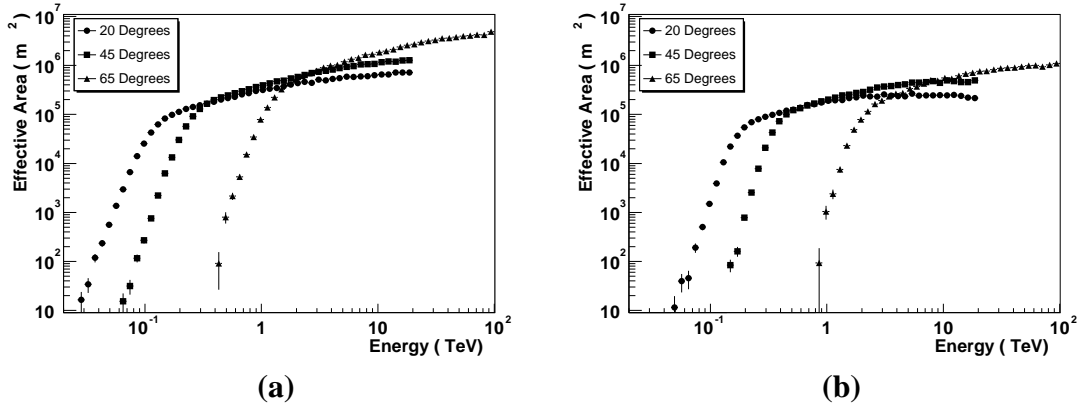


FIGURE 2. The effective collecting area of H.E.S.S. versus energy **a)** before and **b)** after selection cuts for observations at zenith angles of 20°, 45°, and 65°.

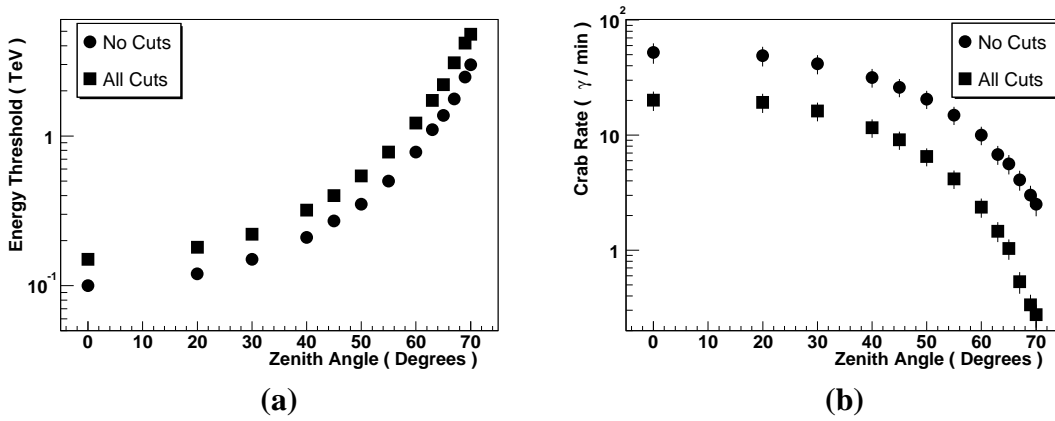


FIGURE 3. **a)** The energy threshold of H.E.S.S. before and after selection cuts versus zenith angle. **b)** The rate of γ -rays expected from a “Crab-like” source before and after selection cuts versus zenith angle.

H.E.S.S. GAMMA-RAY RESPONSE

Using Monte Carlo simulations the effective area of H.E.S.S. is calculated before and after selection cuts, and is shown in Figure 2, for observations at three zenith angles. As can be seen the effective area of H.E.S.S. is significantly larger than the physical size of the detector and increases with energy. The effective area can be convolved with a source energy spectrum to find the expected number of gamma-rays detected by H.E.S.S. versus energy. The peak of this distribution (in equal linear scale intervals of energy) is commonly defined as the energy threshold of the detector. It should be noted that there are photons detected below this energy. Figure 3(a) shows the energy threshold before and after selection cuts for a range of zenith angles calculated using the spectrum of the Crab Nebula ($\Gamma=2.59$, $I_o = 2.79 \times 10^{-7} \text{ m}^{-2} \text{ s}^{-1} \text{ TeV}^{-1}$) as measured by HEGRA[2].

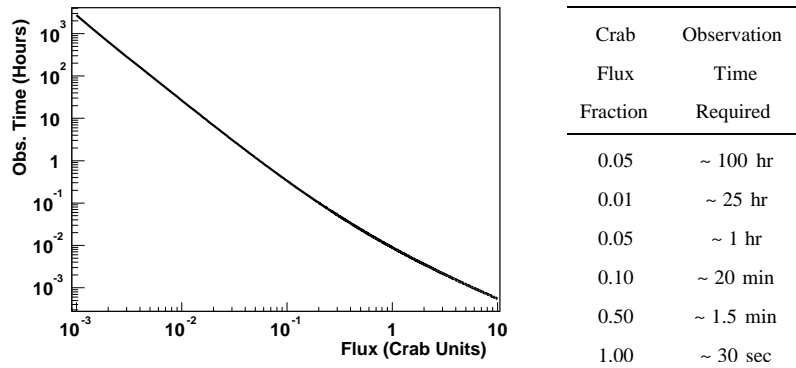


FIGURE 4. The observation time required to yield a 5σ detection at a zenith angle of 20° versus fraction of the Crab flux.

The energy threshold of H.E.S.S. at zenith is 100 GeV before selection cuts and remains below 1 TeV for zenith angles less than 60° where almost all H.E.S.S. observations are performed. The energy threshold is higher after selection cuts due to the minimum size cut applied to the data. Removing this cut lowers the post-selection cuts threshold to the value before cuts, but also lowers the expected significance from a source by $\sim 15\%$. Figure 3(b) shows the expected detection rate of gamma rays from a “Crab-like” source for a range of zenith angles. The rate of detected gamma rays is reasonable even at very large zenith angles allowing H.E.S.S. to perform studies of northern hemisphere sources (such as Mkn 421 and Mkn 501) at multi-TeV energies.

The amount of observation time, at a zenith angle of 20° , required to detect a source for a range of fluxes (assuming the aforementioned HEGRA Crab spectrum) is calculated using the rate of simulated gamma rays passing selection cuts and the post-cuts rate of background events from actual off-source data. The observation time (live hours) required to yield a 5σ detection versus fraction of the HEGRA Crab flux is shown in Figure 4. For comparison to the previous generation of instruments, HEGRA needed ~ 100 hours to detect 5σ from a 5% Crab strength source, where H.E.S.S. would only need 1 hour of observations.

THE CRAB NEBULA

The Crab Nebula is characterized by a relatively large VHE gamma-ray flux that is steady in time and has been seen to energies beyond 20 TeV with no evidence for a cutoff in the source’s power law spectrum. As a result it has been observed by many different instruments and has become the standard reference for gamma-ray astronomy. To verify the performance of H.E.S.S., the Crab Nebula was observed in October 2003 for ~ 2.7 hours (live time) with the three available telescopes at a mean zenith angle of $\sim 47^\circ$. A strong detection is found (52.5σ) and the measured flux and spectrum are consistent with results from other instruments. More details on the H.E.S.S. observations

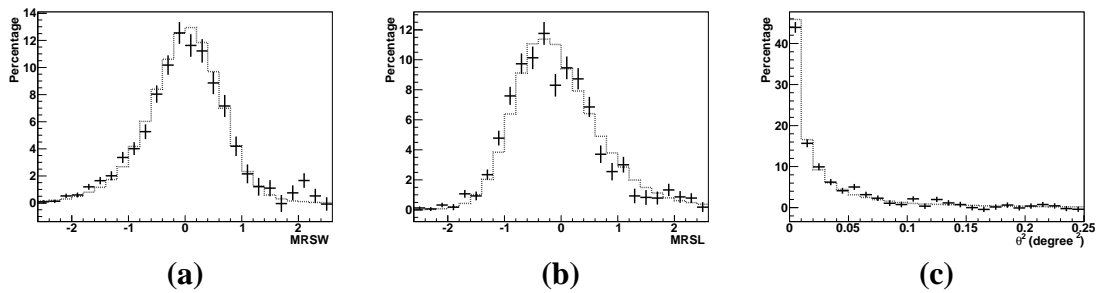


FIGURE 5. The distributions of **a)** mean reduced scaled width (MRSW), **b)** mean reduced scaled length (MRSL), and **c)** θ^2 for the background subtracted signal after selection cuts (excluding both the MRSW and MRSL cuts in (a) and (b), and the θ^2 cut in (c)) from observations of the Crab Nebula (points) and similarly for Monte Carlo gamma-ray simulations ($\Gamma = 2.59$, zenith angle = 45°).

of the Crab Nebula can be found in Masterson *et al.* [7].

Figure 5 shows the distributions of MRSW, MRSL, and θ^2 for the observed excess from the Crab Nebula after all cuts are applied (excluding both the MRSW and MRSL cuts in (a) and (b), and the θ^2 cut in (c)), as well as the corresponding distributions for Monte Carlo gamma-ray simulations. The agreement is good and again verifies that the detector is understood and simulated accurately. In particular, the agreement of the θ^2 distribution demonstrates that the point spread function (width $< 0.1^\circ$) is well understood.

SUMMARY

As of 2004, H.E.S.S. Phase-1 is fully operational and is considerably more sensitive than previous generations of VHE gamma-ray telescopes. The promised sensitivity (1% Crab flux detection in ~ 25 hours) and energy threshold (100 GeV) have been achieved. The detector is well understood and H.E.S.S. has already detected several objects including the Crab Nebula, PKS 2155–304, Mkn 421, the Galactic Center, PSR B1259-63, RXJ 1713.7-3946, and a new source (HESS J1303-631) previously undetected at other wavelengths (all detailed in these proceedings). Other astrophysical objects have been observed for which the analysis is ongoing. Clearly, H.E.S.S. is poised to make further contributions to the field of VHE gamma-ray astronomy.

REFERENCES

1. Aharonian *et al.*, 1999, A&A, 349, 11
2. Aharonian *et al.*, 2000, ApJ, 539, 317
3. Aharonian *et al.*, 2004, Astroparticle Physics, in press (astro-ph/0406658)
4. Bernlöhner *et al.*, 2003, Astroparticle Physics, 20, 111
5. Funk *et al.*, 2004, Astroparticle Physics, in press (astro-ph/0408375)
6. Hofmann, W., 2003, Proc. of the 28th ICRC (Tsukuba), 2811
7. Masterson *et al.*, 2004, these Proceedings
8. Vincent *et al.*, 2003, Proc. of the 28th ICRC (Tsukuba), 2887